(4)

David Taylor Research Center
Bethesda, MD 20084-5000

DTRC-89/030 November 1989
Propulsion and Auxiliary Systems Department
Research and Development Report

Liquid-Metal Flows in Current Collectors for Homopolar Machines: Fully Developed Solutions for the Primary Azimuthal Velocity

by
Gita Talmage
John S. Walker
Samuel H. Brown
Neal A. Sondergaard

DTRC-89/030 Liquid-Metal Flows in Current Collectors for Homopolar Machines: Fully Developed Solutions for the Primary Azimuthal Velocity

MAJOR DTRC TECHNICAL COMPONENTS

CODE 011 DIRECTOR OF TECHNOLOGY, PLANS AND ASSESSMENT

12 SHIP SYSTEMS INTEGRATION DEPARTMENT

14 SHIP ELECTROMAGNETIC SIGNATURES DEPARTMENT

15 SHIP HYDROMECHANICS DEPARTMENT

16 AVIATION DEPARTMENT

17 SHIP STRUCTURES AND PROTECTION DEPARTMENT

18 COMPUTATION, MATHEMATICS & LOGISTICS DEPARTMENT

19 SHIP ACOUSTICS DEPARTMENT

27 PROPULSION AND AUXILIARY SYSTEMS DEPARTMENT

28 SHIP MATERIALS ENGINEERING DEPARTMENT

DTRC ISSUES THREE TYPES OF REPORTS:

1. **DTRC reports, a formal series,** contain information of permanent technical value. They carry a consecutive numerical identification regardless of their classification or the originating department.

2. **Departmental reports, a semiformal series,** contain information of a preliminary, temporary, or proprietary nature or of limited interest or significance. They carry a departmental alphanumerical identification.

3. **Technical memoranda, an informal series,** contain technical documentation of limited use and interest. They are primarily working papers intended for internal use. They carry an identifying number which indicates their type and the numerical code of the originating department. Any distribution outside DTRC must be approved by the head of the originating department on a case-by-case basis.

UNCLASSIFIED

SECURITY CLASSIFICATION OF THIS PAGE

REPORT DOCUMENTATION PAGE

1a. REPORT SECURITY CLASSIFICATION: Unclassified	1b. RESTRICTIVE MARKINGS
2a. SECURITY CLASSIFICATION AUTHORITY	3. DISTRIBUTION/AVAILABILITY OF REPORT: Approved for public release; distribution is unlimited.
2b. DECLASSIFICATION/DOWNGRADING SCHEDULE	
4. PERFORMING ORGANIZATION REPORT NUMBER(S): DTRC-89/030	5. MONITORING ORGANIZATION REPORT NUMBER(S)
6a. NAME OF PERFORMING ORGANIZATION: David Taylor Research Center; 6b. OFFICE SYMBOL (If applicable): Code 2712	7a. NAME OF MONITORING ORGANIZATION
6c. ADDRESS (City, State, and ZIP Code): Bethesda, MD 20084-5000	7b. ADDRESS (City, State, and ZIP Code)
8a. NAME OF FUNDING/SPONSORING ORGANIZATION: IR/IED Program; 8b. OFFICE SYMBOL (If applicable): Code 0120	9. PROCUREMENT INSTRUMENT IDENTIFICATION NUMBER
8c. ADDRESS (City, State, and ZIP Code): Bethesda, MD 20084	10. SOURCE OF FUNDING NUMBERS: PROGRAM ELEMENT NO. 61152N; PROJECT NO. ZR00001; TASK NO. ZR0230201; WORK UNIT ACCESSION NO. 1-2712-125

11. TITLE (Include Security Classification): Liquid-Metal Flows in Current Collectors for Homopolar machines: Fully Developed Solutions for the Primary Azimuthal Vr

12. PERSONAL AUTHOR(S): Gita Talmage, John S. Walker, Samuel H Brown, and Neal A. Sondergaard

13a. TYPE OF REPORT	13b. TIME COVERED	14. DATE OF REPORT (YEAR, MONTH, DAY)	15. PAGE COUNT
Formal	FROM ____ TO ____	November 1989	16

16. SUPPLEMENTARY NOTATION: This report is reprinted from Physics of Fluids A, vol. 1, No. 7 (Jul 1989) pp. 1268-1278. The work was a cooperative effort between DTRC and the Department of Mechanical and Industrial Engineering at the University of Illinois at Urbana 61801

17. COSATI CODES		
FIELD	GROUP	SUB-GROUP

18. SUBJECT TERMS (Continue on reverse if necessary and identify by block number): Current collector, Magnetohydrodynamics, Liquid metal flows, Fluid mechanics, Electrical machinery, Hydrodynamics

19. ABSTRACT (Continue on reverse if necessary and identify by block number)

Liquid metals in the small radial gaps between the rotors and stators of homopolar machines represent low-resistant electric current collectors. Design predictions for these liquid-metal current collectors require a thorough knowledge of liquid-metal flows in a narrow gap between a fixed and a moving surface, with a strong applied magnetic field and a free surface beyond each end of the gap. The radial and axial velocities in the secondary flow are reduce by a strong axial or radial magnetic field. For a sufficiently strong field, the azimuthal momentum transport by the secondary flow can be neglected. This assumption reduces the problem for the primary azimuthal velocity to a fully developed magnetohydrodynamics duct flow problem with a moving wall and two free surfaces. Asymptotic solutions for large Hartmann numbers are presented for skewed magnetic fields with both radial and axial components. Collectors without any electrical insulation or with insulation on the stator sides, or rotor sides, or both are considered. Solutions for a purely axial magnetic field and arbitrary Hartmann numbers are also presented.

20. DISTRIBUTION/AVAILABILITY OF ABSTRACT	21. ABSTRACT SECURITY CLASSIFICATION
☒ UNCLASSIFIED/UNLIMITED ☐ SAME AS RPT ☐ DTIC USERS	Unclassified

22a. NAME OF RESPONSIBLE INDIVIDUAL	22b. TELEPHONE (Include Area Code)	22c. OFFICE SYMBOL
Samuel H. Brown	1-301-267-3458	Code 2712

DD FORM 1473, JUN 86 *Previous editions are obsolete.*

SECURITY CLASSIFICATION OF THIS PAGE

UNCLASSIFIED

0102-LF-014-6602

CREDIT

CONTENTS

FIGURES

ADMINISTRATIVE INFORMATION

This work was a cooperative effort between DTRC and the Department of Mechanical and Industrial Engineering at the University of Illinois, Urbana, Ill. 61801. The work was supported by the DTRC Independent Research Program, Director of Naval Research (OCNR 10), and a administered by the Research Director (DTRC 0113) under program element 61152N, project number ZR00001, task area ZR0230201, work unit 1–2712–125, project title: "Orientation Effects in Liquid Metal Collectors." Also, this work was partially funded by the DTRC Electric Machinery Technology Program under program element 62121N, task area RH21E42, work unit 1–2710–282–10.

Liquid-metal flows in current collectors for homopolar machines: Fully developed solutions for the primary azimuthal velocity

Gita Talmage and John S. Walker
Department of Theoretical and Applied Mechanics, University of Illinois, Urbana, Illinois 61801
Samuel H. Brown and Neal A. Sondergaard
David Taylor Research Center, Bethesda, Maryland 20084-5000

(Received 21 July 1988; accepted for publication 17 February 1989)

Liquid metals in the small radial gaps between the rotors and stators of homopolar machines represent low-resistance electric current collectors. Design predictions for these liquid-metal current collectors require a thorough knowledge of liquid-metal flows in a narrow gap between a fixed and a moving surface, with a strong applied magnetic field and a free surface beyond each end of the gap. The radial and axial velocities in the secondary flow are reduced by a strong axial or radial magnetic field. For a sufficiently strong field, the azimuthal momentum transport by the secondary flow can be neglected. This assumption reduces the problem for the primary azimuthal velocity to a fully developed magnetohydrodynamic duct flow problem with a moving wall and two free surfaces. Asymptotic solutions for large Hartmann numbers are presented for skewed magnetic fields with both radial and axial components. Collectors without any electrical insulation or with insulation on the stator sides, or rotor sides, or both are considered. Solutions for a purely axial magnetic field and arbitrary Hartmann numbers are also presented.

I. INTRODUCTION

In a homopolar generator, the rotation of electrically conducting disks in a strong, axial magnetic field produces a large dc electric current. This current can be used to drive a homopolar motor which has a different applied axial magnetic field strength, a different number of disks, and a different disk radius. This motor-generator combination provides a highly efficient and extremely flexible method of speed reduction, along with other advantages such as maximum torque at zero motor speed. If homopolar devices can be perfected, they will have a number of important applications.[1]

The dc electric current, with a typical current density of 10^7 A/m^2, must flow between the tip of each rotating disk (rotor) and a static current collector (stator) with a minimum voltage drop. State of the art solid brush-slip ring systems,[2] such as silver graphite brushes on a copper slip ring with a protective humidified carbon dioxide atmosphere, typically have contact resistances in the range of 200–600 $\mu\Omega$ at current densities up to $6–7\times10^6$ A/m^2. For larger current densities, the Joulean heating at the interface causes excessive wear. Furthermore, because of the required cooling and mechanical loadings on the brush, it is difficult to achieve packing densities of the brush on the slip ring of greater than 50%–60%. On the other hand, liquid metals, in addition to providing uniform slip ring coverage and essentially wear-free operation, have contact resistances of 1.4 $\mu\Omega$ at 7×10^6 A/m^2. Furthermore, liquid-metal current collectors have been experimentally demonstrated to run for extended periods at an order of magnitude larger current density.[3]

Liquid-metal current collector design predictions require a thorough understanding of the liquid-metal flow in a narrow gap between a moving perfect conductor and a static perfect conductor in the presence of a strong magnetic field and with a free surface beyond each end of the gap. One objective is to predict the voltage difference between the stator and rotor for a given electric current between them. A second objective is to predict and minimize the viscous dissipation and Joulean power losses in the liquid metal. A third objective is to insure that the liquid metal stays in the radial gap at all operating speeds. In present prototypes, an instability occurs at some critical rotation rate and leads to ejection of the liquid metal from the gap. This ejection appears to involve a Kelvin–Helmholtz instability at the free surface due to the difference between the primary azimuthal velocities in the liquid metal and cover gas.[4] The axial gaps between the sides of the rotor and confining radial walls are filled with an inert cover gas from the shaft to the liquid-metal free surface near the rotor tip. Accurate predictions of azimuthal velocities in the liquid metal under various operating conditions are needed to develop stable designs.

A typical value of the magnetic Reynolds number $R_m = \mu_e \sigma UL$ is 0.027. Here, $\mu_e = 4\pi\times10^{-7}$ H/m is the magnetic permeability, $\sigma = 2.38\times10^6$ S/m is the electrical conductivity of a liquid sodium–potassium eutectic mixture at 311 K, $U = \Omega R = 90$ m/sec is the rotor tip velocity, $L = 10^{-4}$ m is the radial gap between the rotor tip and the stator, $\Omega = 300$ rad/sec is the angular velocity, and $R = 0.3$ m is the rotor radius. Therefore, we neglect the magnetic field produced by the electric currents in the liquid metal. The magnetic field in the liquid-metal region consists of the radial and axial magnetic field components, which are produced by superconducting coils around the shaft, and the azimuthal magnetic field component, which is produced by the electric currents in the solid conductors. The magnetic field varies spatially over distances which are comparable to R. Since $L = 3.3\times10^{-4}R$ and a typical axial dimension of the liquid-metal region is $26L = 8.7\times10^{-3}R$, we neglect the

 0899-8213/89/071268-11$01.90

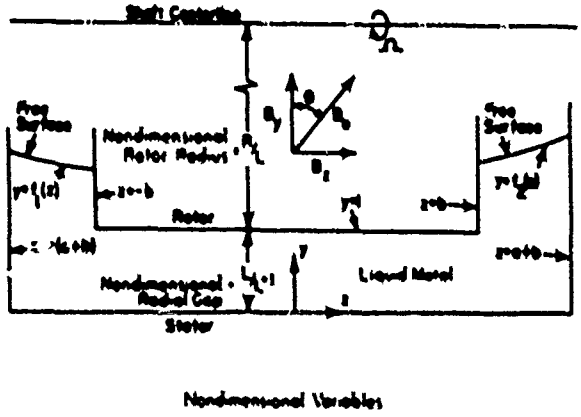

FIG. 1. Liquid-metal region between the stator and rotor. The coordinates and lengths are normalized by the radial gap length L.

variations of the magnetic field components in the small liquid-metal region.

The assumption that $L \ll R$ also means that variations of the radial coordinate are negligible, so that we can use the Cartesian coordinate system shown in Fig. 1. The origin is at the center of the stator, the z axis is parallel to the shaft center line, the y axis points radially inward toward the center line, and the x axis is in the azimuthal direction. The coordinates and lengths are normalized by the radial gap length L, so that $2bL$ is the axial length of the rotor tip, and each axial gap has a length of aL. We use the typical values $b = 10$ and $a = 3$, so that the axial dimension of the liquid-metal region is $26L$. Here, $-B_y$ and B_z represent the radial and axial components of the magnetic field, respectively, while θ is the angle between their resultant and the y axis and $B_{\parallel} = (B_y^2 + B_z^2)^{1/2}$. We need only consider the range $0 \le \theta \le 90°$ because switching the sign of B_z simply reflects the solution about the $z = 0$ plane, while switching the signs of both B_y and B_z simply changes the signs of certain variables.

If the shaft is horizontal, then gravity produces a deviation from an axisymmetric free-surface geometry and solutions. A simple application of lubrication theory indicates that a dimensionless parameter that reflects the relative deviation from an axisymmetric solution is

$$G = \rho g a^2 L^2/\mu U,$$

where $\rho = 867\ \text{kg/m}^3$ and $\mu = 6.5 \times 10^{-3}\ \text{kg/m sec}$ are the density and viscosity of the liquid metal, while $g = 9.81\ \text{m/sec}^2$. A typical value for G is 0.013. Therefore, we neglect gravitational effects and treat only axisymmetric flows in which all variables are independent of x. While gravity produces only a small perturbation of the axisymmetric flow, this small perturbation may play a key role in determining the ejection point in the Kelvin–Helmholtz instability. In a future paper, we will present a perturbation solution for gravitational effects for $G \ll 1$.

While the primary azimuthal velocity u is always comparable to the rotor tip velocity $U = \Omega R$, a strong magnetic field suppresses the secondary flow involving the radial and axial velocities v and w, respectively.[5] A balance between the radial centrifugal force due to the azimuthal velocity and the electromagnetic body force opposing the secondary flow gives a characteristic velocity for the radial and axial velocities, namely

$$U_c \sim \rho \Omega^2 R/\sigma B_{\parallel}^2.$$

The ratio of the characteristic electromagnetic body force that acts on the primary flow, $\sigma \Omega R B_{\parallel}^2$, to the characteristic transport of azimuthal momentum by the secondary flow,

$$\rho\left(v\frac{\partial u}{\partial y} + w\frac{\partial u}{\partial z}\right) \sim \frac{\rho U_c \Omega R}{L},$$

is the interaction parameter

$$N = \sigma^2 B_{\parallel}^4 L/\rho^2 \Omega^2 R$$

with a typical value of 36.2 for $B_{\parallel} = 6$ T. Here, we assume that $N \gg 1$, so that the transport of azimuthal momentum by the secondary flow is neglected. With this assumption, the primary flow is decoupled from the secondary flow and we can determine u independent of v and w. Once u is known, v and w can be determined, where the centrifugal body force $\sim \rho u^2 R^{-1}\hat{y}$, is a known driving force for the secondary flow and $\hat{y}$ is a unit vector. Here, we only present solutions for the primary flow.

The assumption $N \gg 1$ is probably reasonably accurate for $B_{\parallel} = 6$ T, but would not be appropriate for machines with weaker magnetic fields. In a future paper, we will present numerical results for arbitrary N, with full coupling between the primary and secondary flows. The present large-N analytical solutions and the future arbitrary-N numerical solutions are complementary. The analytical solutions are sufficiently simple to treat a wide variety of operating conditions and gain physical insights into the flow phenomena. The numerical solutions, using the approach of Langlois and Walker,[6] are more accurate, particularly for weaker magnetic fields, but require sufficient computer time such that only a few important cases can be treated thoroughly.

Since here we only consider the primary flow, the azimuthal magnetic field B_x plays no role in the solution. The electric currents do interact with B_x to produce pressure variations which influence the free-surface locations, but these effects are part of the secondary flow problem. Here we take the free-surface locations as known.

The Hartmann number

$$M = B_{\parallel} L (\sigma/\mu)^{1/2}$$

has a typical value of 36.3 for $B_{\parallel} = 6$ T. The characteristic ratio of the electromagnetic body force, acting on the primary flow, to the viscous force is M^2. For $M \gg 1$, the liquid-metal region can be divided into the subregions shown in Fig. 2 for axial free surfaces aligned with the rotor tip, i.e., for $f_1(z) = f_2(z) = 1$. Here C1–C3 are the inviscid core regions, H1–H8 are the Hartmann layers with $O(M^{-1})$ thickness which separate the core regions from solid or free surfaces, and F1 and F2 are the interior or free shear layers with $O(M^{-1/2})$ thickness which lie along the two magnetic field lines through the corners where the perfectly conducting rotor tip meets the electrically insulating free surface. Asymptotic treatments of fully developed liquid-metal magnetohydrodynamic (MHD) duct flows for $M \gg 1$ have been

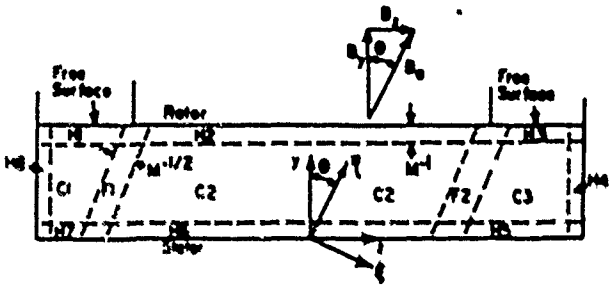

FIG. 2. Subregions of the liquid metal for $M \gg 1$ and the Cartesian coordinates (x,η,ξ), with the η axis parallel to the magnetic field in the x = const plane.

presented in a number of papers published during the 1960's and were thoroughly reviewed by Hunt and Shercliff.[2] The present paper applies this well-established approach to a novel problem of technological importance.

The solution for the geometry shown in Fig. 2 for $M \gg 1$ and $0 < \theta < \arctan(a) = 72°$ is presented in Sec. II. This solution for these special free-surface locations illustrates all the important elements of a large-M asymptotic solution. In Sec. III, we show that the large-M asymptotic analysis is not appropriate for nearly axial magnetic fields and we present a separate, arbitrary-M solution for the axial magnetic field case $\theta = 90°$. In Sec. IV, we extend the analysis to other free-surface locations, $f_1 > 1$ and $f_2 > 1$, with $M \gg 1$ and $\theta < 90°$. In Sec. V, we extend the analysis further to include the cases where the sides of the rotor at $z = \pm b$ or the sides of the stator at $z = \pm (a \pm b)$ are covered with thin layers of an electrical insulator. Since $M^{-1/2} \approx 0.17$ for $B_0 \approx 1$ T is not particularly small and becomes larger for weaker fields, the large-M solutions presented here are only valid for very strong magnetic fields. A future paper will present numerical solutions for arbitrary N and M.

II. AXIAL FREE SURFACES AT THE ROTOR TIP WITH A SKEWED MAGNETIC FIELD

Here we present the asymptotic solution for $M \gg 1$ for $0 < \theta < \arctan(a)$ and $f_1 = f_2 = 1$. It is convenient to use a different set of Cartesian coordinates (x,η,ξ) which have been rotated by an angle θ about the x axis, so that the η axis is parallel to the resultant of the radial and axial magnetic field components, as shown in Fig. 2. The dimensionless governing equations for the primary flow are

$$j_x = M^{-1}\left(\frac{\partial^2 u}{\partial \eta^2} + \frac{\partial^2 u}{\partial \xi^2}\right), \tag{1a}$$

$$j_\eta = -\frac{\partial \phi}{\partial \eta}, \tag{1b}$$

$$j_\xi = -\frac{\partial \phi}{\partial \xi} + u, \tag{1c}$$

$$\frac{\partial j_\eta}{\partial \eta} + \frac{\partial j_\xi}{\partial \xi} = 0, \tag{1d}$$

where u is the azimuthal velocity component normalized by U, j_η and j_ξ are two components of the electric current density normalized by $\sigma U B_{0\eta}$, and ϕ is the deviation of the electric potential function from its value in the perfectly conducting stator normalized by $UB_{0\eta}L$. Equation (1a) is the azimuthal component of the momentum equation for axisymmetric flow, with negligible azimuthal momentum transport by the secondary flow; Eqs. (1b) and (1c) are the η and ξ components of Ohm's law; and Eq. (1d) is the conservation of current equation.

Since ϕ is the dimensionless deviation from the electric potential in the stator, the boundary conditions at all three stator surfaces are

$$u = 0, \tag{2a}$$

$$\phi = 0. \tag{2b}$$

Since the rotor is a perfect conductor moving through a magnetic field, the boundary conditions at the rotor face are

$$u = 1, \tag{3a}$$

$$\phi = \phi_0 + \sin\theta \cdot \xi = \Psi(\xi), \tag{3b}$$

where ϕ_0 is the dimensionless potential at the center of the rotor face, i.e., at $y = 1$, $z = 0$, or $\eta = \cos\theta$, $\xi = -\sin\theta$. The dimensional voltage difference between the rotor and stator at their midplane $z = 0$, is $\phi_0 UB_{0\eta}L$. We assume that the cover gas is an electrical insulator with negligible shear stresses, so that the boundary conditions at both free surfaces are

$$\frac{\partial u}{\partial y} = 0, \tag{4a}$$

$$j_y = 0. \tag{4b}$$

In the three core regions C1–C3, all derivatives are $O(1)$, so that the solution of Eqs. (1) is

$$j_{\xi c} = 0, \tag{5a}$$

$$\phi_c = \psi_c - \eta j_{\eta c}, \tag{5b}$$

$$u_c = \frac{\partial \phi_c}{\partial \xi}, \tag{5c}$$

neglecting $O(M^{-2})$ terms. Here, $\psi_c(\xi)$ and $j_{\eta c}(\xi)$ are integration functions which are determined by matching the Hartmann layer solutions. The Hartmann layers adjacent to the stator or rotor surfaces satisfy the boundary conditions (2a) and (3a) and match any core velocity. The Hartmann layer structure that accommodates a jump in the $O(1)$ u leads to an $O(M^{-1})$ jump in the electric potential across the layer for any perfectly conducting wall whose surface is not perpendicular or parallel to the magnetic field vector. Since the maximum jump in ϕ is $O(M^{-1})$, the conditions (2b) and (3b) can be applied directly to the $O(1)$ core solutions. For the Hartmann layers adjacent to the two free surfaces, the $O(1)$ u is continuous through the layer. The boundary layer structure develops if the $O(1)$ value of $\partial u/\partial y$ in the core is not zero at $y = 1$. This structure involves a jump in the $O(M^{-1})$ velocity and the $O(M^{-2})$ normal electric current density j_y. Therefore, the boundary condition (4b) can be applied to the $O(1)$ and $O(M^{-1})$ variables in the core regions C1 and C3.

For the core regions C1 and C3, the solution (5) that satisfies the Hartmann layer jump conditions is

$$j_{\xi c} = 0, \tag{6a}$$

$$j_{\eta c} = 0, \tag{6b}$$

$$\phi_{x} = 0, \tag{6c}$$

$$u_{x} = 0, \tag{6d}$$

neglecting $O(M^{-2})$ terms. The boundary condition (2b) is applied to the $O(1)$ and $O(M^{-1})$ potentials ϕ because there is no jump in the $O(1)$ u across any of the stator Hartmann layers H4, H5, H7, and H8. In the core C2, the $O(1)$ variables are

$$j_{\psi 2} = -\cos\theta\Psi, \tag{7a}$$

$$\phi_{x2} = (\eta\cos\theta - \xi\sin\theta)\Psi, \tag{7b}$$

$$u_{x2} = \eta\cos\theta - \sin\theta(\Psi + \xi), \tag{7c}$$

where the rotor-surface potential $\Psi(\xi)$ is defined by Eq. (3b). The $O(M^{-1})$ variables in core C2 are easily obtained by matching the jump conditions for the Hartmann layers H2 and H6, but these variables are not presented here because they represent minor corrections. The core solution (7) holds in the region defined by

$$0 < \eta - \xi\tan\theta < \sec\theta, \quad \text{for } |\xi + \sin\theta| < b\cos\theta.$$

The core regions C1 and C3 are stagnant, current-free regions. The core C2 involves an $O(1)$ current density which is parallel to the magnetic field and equal to the local potential difference between the stator and rotor $\Psi(\xi)$ divided by the distance between the stator and rotor along a magnetic field line $\sec\theta$. The first term in the velocity solution (7c) represents linear Couette flow and the second term is an additional velocity associated with the current flow. This additional velocity is independent of η, linear in ξ, decreases linearly as ϕ_0 is increased, and vanishes for a purely radial magnetic field $\theta = 0$. We discuss the core solutions further after we present the free shear layer solutions.

The core solutions (6c) and (7b) indicate that each free shear layer must accommodate a jump in the $O(1)$ potential ϕ. The magnitude of this jump increases linearly from zero at the stator to $\phi_1 = \phi_0 - b\cos\theta$ or $\phi_2 = \phi_0 + b\cos\theta$ at the rotor corner for the free shear layer F1 or F2, respectively. With an $O(1)$ potential ϕ, Eq. (1b) implies that j_{η} is $O(1)$ as well. Since $\partial/\partial\xi = O(M^{1/2})$ inside a free shear layer, Eq. (1d) implies that j_{ξ} is $O(M^{-1/2})$. Equation (1c) then implies that u is very large, namely $O(M^{1/2})$. The first and last terms in Eq. (1a) now balance, which is why the free shear layer thickness is $O(M^{-1/2})$. We consider only F1 because its solution reduces to a universal solution which applies for layer F2 and any similar free shear layer.

For the free shear layer F1, we rescale the dependent and independent variables by substituting

$$\phi = \phi_1\phi_f(t,\zeta) + O(M^{-1/2}), \tag{8a}$$

$$u = M^{1/2}\phi_1\lambda^{-1/2}u_f(t,\zeta) + O(1), \tag{8b}$$

$$j_{\eta} = \phi_1\lambda^{-1}j_{\psi f}(t,\zeta) + O(M^{-1/2}), \tag{8c}$$

$$j_{\xi} = M^{-1/2}\phi_1\lambda^{-3/2}j_{\xi f}(t,\zeta) + O(M^{-1}), \tag{8d}$$

$$t = (\eta + b\sin\theta + \tan\theta\sin\theta)\lambda^{-1}, \tag{8e}$$

$$\zeta = M^{1/2}(\xi + \sin\theta + b\cos\theta)\lambda^{-1/2}, \tag{8f}$$

where $\lambda = \sec\theta$ is the length of the free shear layer from the stator to the rotor corner. The coordinate t is a local rescaling of the η coordinate, so that $t = 0$ at the stator and $t = 1$ at the rotor corner. The coordinate ζ is the stretched local ξ coordinate, so that the free shear layer solution matches the C1 or C2 core solution as $\zeta \to -\infty$ or $\zeta \to \infty$, respectively. With the factors involving ϕ_1 and λ in Eqs. (8), the free shear layer variables ϕ_f, u_f, $j_{\psi f}$, and $j_{\xi f}$ are universal functions of the rescaled coordinates (t,ζ) and are completely independent of the parameters ϕ_0, θ, a, and b. With the substitutions (8), the leading terms in Eqs. (1) become

$$j_{\xi f} = \frac{\partial^2 u_f}{\partial\zeta^2}, \tag{9a}$$

$$j_{\psi f} = -\frac{\partial\phi_f}{\partial t}, \tag{9b}$$

$$u_f = \frac{\partial\phi_f}{\partial\zeta}, \tag{9c}$$

$$\frac{\partial^2\phi_f}{\partial t^2} = \frac{\partial^4\phi_f}{\partial\zeta^4}. \tag{9d}$$

There are Hartmann layers with $O(M^{-1})$ thickness which separate the free shear layer from the stator, rotor, and free surface. The jump in ϕ across the Hartmann layers adjacent to the stator and rotor is again $O(M^{-1})$, so that the boundary conditions (2b) and (3b) can be applied to the $O(1)$ free shear layer ϕ. The jump in j_x across the free-surface Hartmann layer is $O(M^{-1})$, so that the boundary condition (4b) can be applied to the $O(1)$ free shear layer current density. These conditions become

$$\phi_f = 0, \quad \text{at } t = 0, \quad \text{for } -\infty < \zeta < \infty, \tag{10a}$$

$$\phi_f = 1, \quad \text{at } t = 1, \quad \text{for } 0 < \zeta < \infty, \tag{10b}$$

$$\frac{\partial\phi_f}{\partial t} = 0, \quad \text{at } t = 1, \quad \text{for } -\infty < \zeta < 0. \tag{10c}$$

Matching the core solutions (6c) and (7b) gives

$$\phi_f \to 0, \quad \text{as } \zeta \to -\infty, \tag{11a}$$

$$\phi_f \to t, \quad \text{as } \zeta \to \infty. \tag{11b}$$

Once we find the solution ϕ_f that satisfies Eq. (9d) and the conditions (10) and (11), the other variables are given by Eqs. (9a)–(9c).

The separation of variables solution of Eq. (9d) for $-\infty < \zeta < 0$, which satisfies conditions (10a), (10c), and (11a), is

$$\phi_f = \sum_{m=0}^{\infty}\sin(2\alpha_m^2 t)e^{\alpha_m\zeta}[A_m\cos(\alpha_m\zeta) + B_m\sin(\alpha_m\zeta)], \quad \text{for } -\infty < \zeta < 0, \tag{12}$$

where

$$\alpha_m = [\tfrac{1}{2}(2m+1)\pi]^{1/2}.$$

The corresponding separation of variables solution for $0 < \zeta < \infty$, which satisfies conditions (10a), (10b), and (11b), is

$$\phi_f = t + \sum_{n=1}^{\infty}\sin(n\pi t)e^{-\beta_n\zeta}[C_n\cos(\beta_n\zeta) + D_n\sin(\beta_n\zeta)], \quad \text{for } 0 < \zeta < \infty, \tag{13}$$

where

$$\beta_n = (\tfrac{1}{2}n\pi)^{1/2}.$$

The constants A_m, B_m, C_n, and D_n are determined by the four conditions that ϕ_f and its first three derivatives with

respect to ζ are continuous at $\zeta = 0$. The governing equation (9d) then ensures that all derivatives with respect to ζ are continuous at $\zeta = 0$. Since the Fourier series in the solutions (12) and (13) are not orthogonal to each other, we truncate both series and define a residual from the conditions at $\zeta = 0$:

$$E = \int_{t_0}^{1} \sum_{n=0}^{4} \left(\frac{\partial^n \phi_F}{\partial \zeta^n}(t,0^-) - \frac{\partial^n \phi_F}{\partial \zeta^n}(t,0^+) \right)^2 dt,$$

where the truncated solutions (12) and (13) are used to compute values at $\zeta = 0^-$ and at $\zeta = 0^+$, respectively. This residual is minimized with respect to the constants A_m, B_m, C_n, and D_n and this minimization gives a set of simultaneous, linear, algebraic equations for these constants. These equations are solved with Gauss elimination and the truncated series (12) and (13) are used to compute the other free shear layer variables from Eqs. (9a)–(9c).

The profiles of u_F at $t = 0.2, 0.4, 0.6, 0.8, 0.94$, and 1.0 are presented in Fig. 3. At $t = 1.0$, (i) $u_F < 0$ for $-6 < \zeta < -2.9$, (ii) u_F increases rapidly from zero at $\zeta = -2.9$ to 0.7 at $\zeta = 0$, and (iii) u_F has a discontinuity at $\zeta = 0$ after which $u_F = 0$ for $\zeta > 0$. For $\zeta < -0.1$, the profiles at $t = 0.94$ and 1.0 are very close. However, the discontinuity at $\zeta = 0$ for $t = 1.0$ is replaced by a rapid decrease between $\zeta = -0.1$ and $\zeta = 0.9$ for $t = 0.94$. At $t = 0.94$, $u_F < 0$ for $0.9 < \zeta < 2$. As t decreases from 0.94, the peak velocity decreases to 0.423 at $\zeta = -0.44$ for $t = 0.8$, to 0.278 at $\zeta = -0.5$ for $t = 0.6$, to 0.174 at $\zeta = -0.53$ for $t = 0.4$, and to 0.084 at $\zeta = -0.56$ for $t = 0.2$. In addition, the velocity profiles spread out as t decreases. Equation (9c) and conditions (11) show that

$$\int_{-\infty}^{0} u_F \, d\zeta = t,$$

so that the flow carried by each of the profiles in Fig. 3 is proportional to t.

Walker *et al.*[8,9] treat a similar free shear layer with the present free surface replaced by a solid electrical insulator. Their boundary value problem is the same as the present problem (9)–(11) except that the free-surface condition (10c) is replaced by

$$\frac{\partial \phi_F}{\partial t} = \frac{\partial^2 \phi_F}{\partial \zeta^2}, \quad \text{at } t = 1, \quad \text{for } -\infty < \zeta < 0, \tag{14}$$

which is the Hartmann layer matching condition at the solid insulator. This difference precludes the use of the present separation of variables solutions. With a solid insulator, a Fourier transform reduces the problem to an integral equation which must be solved numerically.[9] In spite of the fact that the problem with a solid insulator requires a much more complex solution technique, the results for the velocity profiles and the other variables are very similar to the present results.

The solution in the free shear layer F2 in terms of the same universal functions u_F, ϕ_F, j_{yF}, and $j_{\zeta F}$ is

$$\phi = \phi_2 \phi_F(t,\zeta) + O(M^{-1/2}), \tag{15a}$$

$$u = -M^{1/2} \phi_2 \lambda^{-1/2} u_F(t,\zeta) + O(1), \tag{15b}$$

$$j_y = \phi_2 \lambda^{-1} j_{yF}(t,\zeta) + O(M^{-1/2}), \tag{15c}$$

$$j_\zeta = -M^{1/2} \phi_2 \lambda^{-1/2} j_{\zeta F}(t,\zeta) + O(M^{-1}), \tag{15d}$$

$$t = (\eta + \sin\theta \tan\theta - b \sin\theta)\lambda^{-1}, \tag{15e}$$

$$\zeta = -M^{1/2}(\xi + \sin\theta - b\cos\theta)\lambda^{-1/2}. \tag{15f}$$

Here, the potential jump across the free shear layer increases linearly from zero at the stator to $\phi_2 = \phi_0 + b\cos\theta$ at the rotor corner, while $\lambda = \sec\theta$ is the length of the layer from the stator to the rotor.

For no net electric current between the stator and rotor, $\phi_0 = 0$, $\phi_1 = -b\cos\theta$, and $\phi_2 = b\cos\theta$. The solutions (8b) and (15b) indicate that the free shear layers are identical jets in the $-x$ direction for this case. The rotor tip and liquid metal in the free shear layers are going in opposite azimuthal directions. The velocity at the free surface very near each rotor corner is approximately $-0.7M^{1/2}b(\cos\theta)^{1/2}$. As ϕ_0 is increased from zero to drive a net current from the rotor to the stator, the free shear layer F2 becomes a stronger jet in the $-x$ direction, while layer F1 decreases in strength to zero flow at $\phi_0 = b\cos\theta$. For $\phi_0 > b\cos\theta$, layer F1 becomes a jet in the $+x$ direction. As ϕ_0 is decreased from zero to drive a net current from the stator to rotor, the above description of layer F1 applies to layer F2 and vice versa.

For core C2, the net dimensionless electric current from the rotor to the stator, per unit Δz, is

$$2\phi_0 b\cos^2\theta. \tag{16}$$

Equation (16) is multiplied by $2\pi\sigma UB_0LR$ to obtain the net dimensional current from the rotor to the stator. As θ increases from zero, the electrical resistance of the liquid-metal region increases as $\sec^2\theta$. This is because the length of the current lines increases as $\sec\theta$, while the area perpendicular to the current direction decreases as $\cos\theta$. The core regions C1 and C3 carry no current. The two free shear layers allow a small additional current to flow between the stator and rotor because electric current lines are allowed to fringe an $O(M^{-1/2})$ distance beyond the lines $\xi = -\sin\theta \pm b\cos\theta$. However, the ratio of this additional free shear layer current to the C2 core current is comparable to $M^{-1/2}b^{-1}(\sec\theta)^{3/2}$.

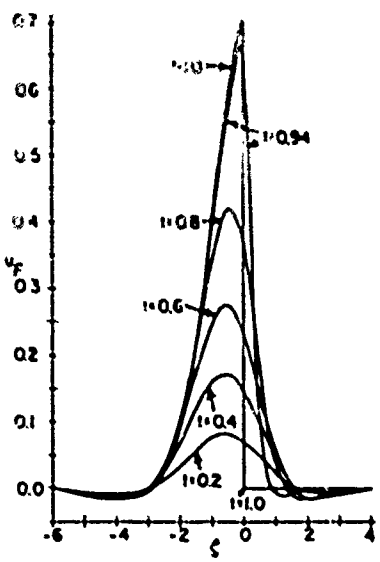

FIG. 3. Free shear layer velocity u_F at $t = 0.2, 0.4, 0.6, 0.8, 0.94$, and 1.0.

This ratio is quite small, except as θ approaches 90°, which is the case treated in Sec. III. While the current-line fringing inside the free shear layers does not significantly increase the net current, it does produce a small $O(M^{-1/2})$ electric current component perpendicular to the magnetic field. The electromagnetic body force due to this small j_z drives the jets with $O(M^{1/2})$ u inside the free shear layers.

Here we present the $O(M^{-2})$ and $O(M^{-1/2})$ dimensionless power losses due to Joulean heating and viscous dissipation, per unit Δx. Total dimensional power losses are obtained by multiplying each result by $2\pi R_0 U^2$. The only $O(M^{-2})$ dimensionless power loss is the Joulean heating in the core C2. This loss is given by the integral of the square of solution (7a) over the core region and the result is

$$\tfrac{1}{4}M^{-2}\cos\theta(\phi_2^+ - \phi_1^+) \tag{17}$$

The $O(M^{-1/2})$ contributions to the power losses are (i) the viscous dissipation due to the large gradient of the large velocity in each free shear layer and (ii) the Joulean heating due to the fringing of the $O(1)$ electric current density inside the free shear layers. With the solutions (8) and (15), these power losses are given by coefficients times integrals of $(\partial u_f/\partial\xi^*)^2$ and $j_{\xi f}^2$ over the region $0 < \eta < 1$, $-\infty < \xi < \infty$. Since these universal functions are independent of all parameters, these integrals give sums of the known coefficients in the separation of variables solutions (12) and (13). These sums give specific numerical values which apply to all similar free shear layers. The results for the dimensionless viscous dissipation and Joulean heating are

$$0.131M^{-1/2}\phi_*^2\lambda^{-1/2}, \tag{18a}$$

$$0.407M^{-1/2}\phi_*^2\lambda^{-1/2}, \tag{18b}$$

respectively, where ϕ_* is ϕ_1 or ϕ_2 for layer 1-1 or 1-2.

III. AXIAL MAGNETIC FIELD

The solutions in Sec. II apply for $0 < \theta < \arctan(a) = 72°$ for $a = 3$. For a purely axial magnetic field, $\theta = 90°$, $B_r = 0$, and $B_z = B_0$, and we use the original (x,y,z) Cartesian coordinates shown in Fig. 2. With the same nondimensionalization, Eqs. (1) are replaced by

$$0 = j_x + M^{-1}\left(\frac{\partial^2 u}{\partial y^2} + \frac{\partial^2 u}{\partial z^2}\right), \tag{19a}$$

$$j_y = -\frac{\partial\phi}{\partial z}, \tag{19b}$$

$$j_z = -\frac{\partial\phi}{\partial y} + u, \tag{19c}$$

$$\frac{\partial j_y}{\partial y} + \frac{\partial j_z}{\partial z} = 0. \tag{19d}$$

The flow is now symmetric about the $z = 0$ plane, so that we need only solve Eqs. (19) for $0 < y < 1$ and $0 < z < a + b$. The boundary conditions are

$$u = 0, \quad \text{at } y = 0, \tag{20a}$$

$$\phi = 0, \quad \text{at } y = 0, \tag{20b}$$

$$\frac{\partial u}{\partial z} = 0, \quad \text{at } z = 0, \tag{20c}$$

$$\frac{\partial\phi}{\partial z} = 0, \quad \text{at } z = 0, \tag{20d}$$

$$u = 0, \quad \text{at } z = a + b, \tag{20e}$$

$$\phi = 0, \quad \text{at } z = a + b, \tag{20f}$$

$$u = 1, \quad \text{at } y = 1, \quad \text{for } 0 < z < b, \tag{20g}$$

$$\phi = \phi_w, \quad \text{at } y = 1, \quad \text{for } 0 < z < b, \tag{20h}$$

$$\frac{\partial u}{\partial y} = 0, \quad \text{at } y = 1, \quad \text{for } b < z < a + b, \tag{20i}$$

$$j_z = 0, \quad \text{at } y = 1, \quad \text{for } b < z < a + b. \tag{20j}$$

Since the magnetic field is now parallel to the rotor surface, this surface is at a single dimensionless electric potential ϕ_w.

In the asymptotic solution for $M \gg 1$, $u = \phi = j_z = j_y = 0$ to all orders in M, except in a thin boundary layer which has an $O(M^{-1/2})$ thickness and is adjacent to the free and rotor surfaces at $y = 1$. All the electric current from the stator to the rotor flows axially inside this layer near the free surfaces and enters the rotor near the corners. The azimuthal velocity u is $O(M^{1/2})$ inside this layer. In other words, as $\theta \to 90°$, the two free shear layers from the rotor corners merge to become a free-surface, rotor-face boundary layer; the current-carrying core C2 disappears; and the stagnant, current-free core C3 expands to fill most of the liquid-metal region. However, the large-M asymptotic solution is not appropriate for an axial or nearly axial magnetic field in homopolar devices.

Figure 3 shows that the jets in the free shear layers are confined to $1 - \xi < 1$, so that Eq. (8f) indicates that the free shear layer thickness is $4\lambda^{-1/2}M^{-1/2}$. For $\theta < \arctan(a)$, the length of each free shear layer is $\lambda = \sec\theta$. The ratio of the free shear layer thickness to the $\Delta\xi = 2b\cos\theta$ of core C2 is

$$2(\sec\theta)^{-1/2}M^{-1/2}b^{-1}.$$

The large-M asymptotic analysis is appropriate for $0 < \theta < \arctan(a)$ as long as the above ratio is small. For $\theta = 45°$, $M = 36.3$, and $b = 10$, the ratio is 0.056. For the axial field case, λ becomes the entire length of the $O(M^{-1/2})$ thickness layer adjacent to $y = 1$, so that $\lambda = 2(a + b)$. Assuming $\Delta\xi$ is still 4, the ratio of the Δy of this layer to the entire $\Delta y = 1$ is

$$4[2(a + b)/M]^{1/2};$$

this ratio must be small for the large-M asymptotic solution to be valid for the axial field case. For $a = 3$, $b = 10$, and $M = 36.3$ this ratio is 3.39. Therefore, viscous effects are significant everywhere and we must treat M as an $O(1)$ parameter.

We introduce the electric current streamfunction $h(y,z)$, which is defined by

$$j_y = M^{-1}\frac{\partial h}{\partial z}, \tag{21a}$$

$$j_z = -M^{-1}\frac{\partial h}{\partial y}. \tag{21b}$$

Since j_y and j_z are even and odd functions of z, respectively, h is an odd function of z. We eliminate ϕ from Eqs. (19b) and (19c), so that Eqs. (19) become

$$\frac{\partial^2 u}{\partial y^2} + \frac{\partial^2 u}{\partial z^2} + M\frac{\partial h}{\partial z} = 0, \tag{22a}$$

$$\frac{\partial^2 h}{\partial y^2} + \frac{\partial^2 h}{\partial z^2} + M \frac{\partial u}{\partial z} = 0. \tag{22}$$

The boundary conditions (20a), (20c), (20e), (20g), and (20i) on u still apply, but the conditions (20h), (20d), (20f), (20h), and (20j) on ϕ are replaced by

$$\frac{\partial h}{\partial y} = 0, \quad \text{at } y = 0, \tag{23a}$$

$$h = 0, \quad \text{at } z = 0, \tag{23b}$$

$$\frac{\partial h}{\partial z} = 0, \quad \text{at } z = a + b, \tag{23c}$$

$$\frac{\partial h}{\partial y} = 0, \quad \text{at } y = 1, \quad \text{for } 0 < z < b, \tag{23d}$$

$$h = h_0, \quad \text{at } y = 1, \quad \text{for } b < z < a + b. \tag{23e}$$

The constant h_0 is proportional to the total dimensional electric current from the stator to the rotor, which is

$$4\pi h_0 M^{-1} \sigma U B_0 R L = 4\pi h_0 U R (\sigma\mu)^{1/2}.$$

Once the solutions for u and h are known, we introduce them into Eq. (19c) and integrate with respect to y to obtain $\phi(y,z)$ and ϕ_0.

Equations (22) and the boundary conditions (20a), (20c), (20e), and (23a)–(23c), except at $y = 1$, are satisfied by the separation of variables solutions

$$u = -\sum_{n=0}^{\infty} \cos(\delta_n z) \left[G_n F_{1n} + H_n \left(F_{2n} + \frac{m_r}{m_i} F_{3n} \right) \right], \tag{24a}$$

$$h = \sum_{n=0}^{\infty} \sin(\delta_n z) \left[G_n F_{4n} + H_n \left(F_{3n} - \frac{m_r}{m_i} F_{2n} \right) \right], \tag{24b}$$

where G_n and H_n are arbitrary constants and

$$\delta_n = (2n + 1)\pi/2(a + b), \tag{24c}$$

$$m_r = (2)^{-1/2} \delta_n \left[(1 + M^2 \delta_n^{-2})^{1/2} + 1 \right]^{1/2}, \tag{24d}$$

$$m_i = (2)^{-1/2} \delta_n \left[(1 + M^2 \delta_n^{-2})^{1/2} - 1 \right]^{1/2}, \tag{24e}$$

$$F_{1n} = \sinh(m_r y)\sin(m_i y), \tag{24f}$$

$$F_{2n} = \cosh(m_r y)\sin(m_i y), \tag{24g}$$

$$F_{3n} = \sinh(m_r y)\cos(m_i y), \tag{24h}$$

$$F_{4n} = \cosh(m_r y)\cos(m_i y). \tag{24i}$$

The constants G_n and H_n are determined by the remaining boundary conditions (20g), (20i), (23d), and (23e) at $y = 1$. We truncate the series and define a residual

$$E = \int_0^b \left[(u - 1)^2 + \left(\frac{\partial h}{\partial y} \right)^2 \right] dz + \int_b^{a+b} \left[\left(\frac{\partial u}{\partial y} \right)^2 + (h - h_0)^2 \right] dz, \tag{25}$$

where the integrands are given by the series (24) evaluated at $y = 1$. When the residual (25) is minimized with respect to the constants G_n and H_n, it gives a set of simultaneous, linear, algebraic equations for these constants. These equations are solved using Gauss elimination.

Some typical results for $a = 3$, $b = 10$, $M = 40$, and $h_0 = \pm 10$ are presented in Fig. 4. The y scale is stretched by a factor of 5 relative to the z scale. Figures 4(a) and 4(c) show that electric current prefers to flow axially along the magnetic field lines near the free surface, rather than flow across the field lines in the central part of the radial gap. For $h_0 = 10$ or -10, 78% or 60% of the total current leaves or enters the stator side at $z = a + b$, rather than the axial surface at $y = 0$. For current from the stator to the rotor, Fig. 4(b) shows that the maximum velocity is $u = 3.13$ near the rotor corner. For current from the rotor to the stator, Fig. 4(d) shows that the minimum velocity at the free surface is $u = -1.4$ near the rotor corner, but the minimum velocity is $u = -2$ near $y = 0.5$ for $0 < z < 6$.

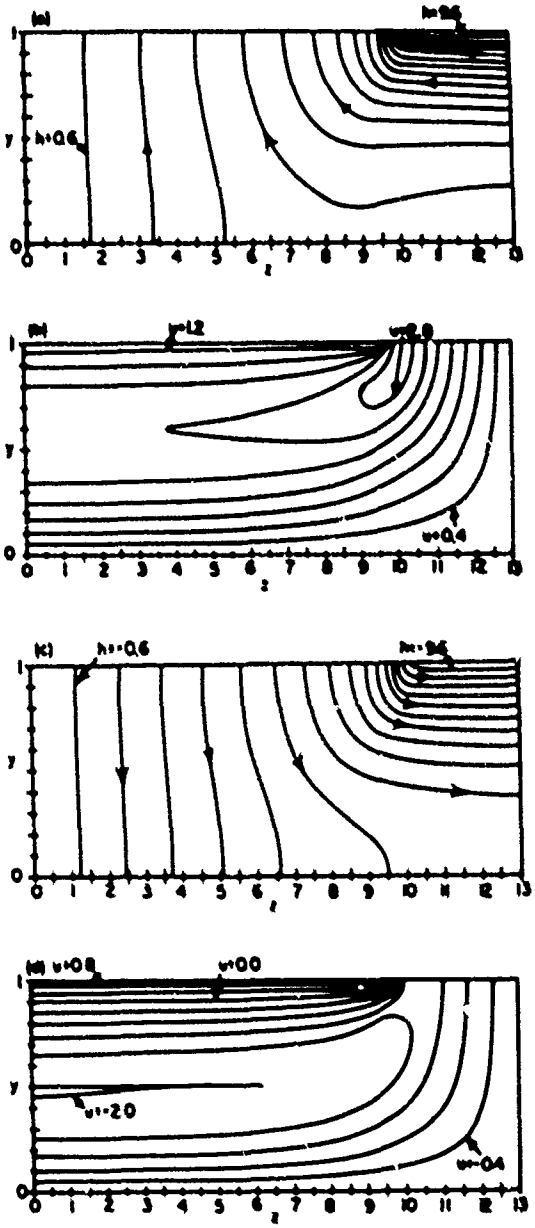

FIG. 4. Electric current lines h = const and velocity magnitude lines u = const for an axial magnetic field with $a = 3$, $b = 10$, and $M = 40$. (a) Current lines for $h_0 = 10$, (b) velocity magnitudes for $h_0 = 10$, (c) current lines for $h_0 = -10$, and (d) velocity magnitudes for $h_0 = -10$.

In a homopolar device, there are two groups of rotors or disks which are separated axially along the shaft. Each disk in one group is electrically connected along the shaft with

one disk in the other group. Electric current flows radially inward inside all the disks in one group and radially outward inside all the disks in the other group. The magnet coils create axial magnetic fields in opposite directions for the two groups of disks. Therefore, the electromagnetic body force is in the same azimuthal direction in all the disks in both groups. The analysis here assumes that the disk's angular velocity vector and the axial magnetic field are in the same direction, i.e., that $U = \Omega R > 0$ and $B_a > 0$. For the present solution, if we replace $B_z = B_0$ with $B_z = -B_0$ and we replace h by $-h$, then the velocities are exactly the same. In addition, the electric currents are exactly the same, but are in the opposite direction. The results for $h_0 > 0$ apply for current from the stator to the rotor for $B_z > 0$ and for current from the rotor to the stator for $B_z < 0$ and vice versa for $h_0 < 0$. Therefore, $h_0 > 0$ corresponds to all liquid-metal current collectors in a homopolar motor. In a motor, the electromagnetic body force in the disks and liquid metal is in the direction of rotation, so that u is increased to $u > 1$, as shown in Fig. 4(b). On the other hand, $h_0 < 0$ corresponds to all current collectors in a homopolar generator. In a generator, the azimuthal electromagnetic body force in the disks and liquid metal is in the opposite azimuthal direction from the disk rotation, so that u is decreased to $u < 0$, as shown in Fig. 4(d).

The value of ϕ_0 is a linear function of h_0. For example, for $a = 3$, $b = 10$, and $M = 10$,

$$\phi_0 = -0.456 - 0.082\,43 h_0.$$

The total Joulean heating and viscous dissipation are parabolic functions of h_0. For example, for $a = 3$, $b = 10$, and $M = 10$, the dimensionless total Joulean heating and viscous dissipation are

$$2.736 + 0.954 h_0 + 0.2909 h_0^2,$$

$$21.65 - 0.984 h_0 + 1.343 h_0^2,$$

respectively. Total dimensional power losses are obtained by multiplying each result by $2\pi R\mu U^2$.

IV. GENERAL FREE-SURFACE LOCATIONS AND A STRONG, SKEWED MAGNETIC FIELD

Here we present the extension of the large-M asymptotic analysis for a skewed magnetic field to general free-surface locations at $y = f_1(z)$ for $-a - b < z < -b$ and at $y = f_2(z)$ for $b < z < a + b$, as shown in Fig. 5. The solution (6) still applies in core regions C1 and C3. The electric potential of all rotor surfaces is $\Psi(\xi) = \phi_0 + \sin\theta + \xi$. In core C2, the solution in the radial gap is still given by the results (7) for $|\xi + \sin\theta| < b\cos\theta$. For $-b\cos\theta - f(-b)\sin\theta < \xi < -b\cos\theta - \sin\theta$, ϕ_c is a linear function of η, which equals zero at the stator and $\Psi(\xi)$ at the rotor, while j_{yc} and u_c are given by Eqs. (1b) and (5c), respectively. There is a weak free shear layer at $\xi = -\sin\theta - b\cos\theta$ along the magnetic field line through the corner at $y = 1$, $z = -b$. The electric potential is continuous across this layer, but u_c is discontinuous between the two parts of core C2. The free shear layer structure that matches this jump in u_c involves only an $O(1)$ velocity, so that it is a much weaker layer than

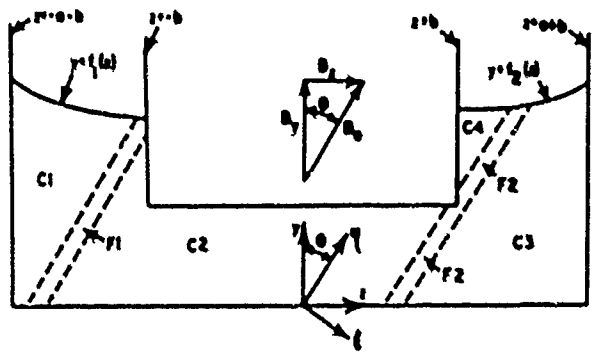

FIG. 5. Subregions of the liquid metal for $M \gg 1$ and general free-surface locations. The Hartmann layers and a weak free shear layer at $\xi = -\sin\theta - b\cos\theta$ are not shown.

layers F1 and F2, which involve an $O(M^{-1/2})$ velocity. In core C4,

$$\phi_c = \Psi(\xi), \quad u_c = 1, \quad j_{yc} = j_{\xi c} = 0, \tag{26}$$

neglecting $O(M^{-1})$ terms.

The solution in the free shear layer F1 is given by expressions (8) in terms of the same universal functions ϕ_f, u_f, j_{yf}, and $j_{\xi f}$, but now λ is the free shear layer length from the stator to the point where the free surface and rotor side meet at $y = f_1(-a - b)$, $z = -a - b$, while

$$\phi_0 = \phi_{i0} + \sin\theta\,[1 + f_1'(-a - b)]\,(-a - b)\cos\theta$$

is Ψ at this point.

For the free shear layer F2, we again rescale the dependent and independent variables by introducing expressions (15) with $\lambda = \sec\theta$ and $\phi_2 = \phi_{i0} + b\cos\theta$. However, the functions ϕ_f, u_f, j_{yf}, and $j_{\xi f}$ are not the same functions as before; thus we add the subscript 2 to denote these new functions. These rescaled variables are functions of (t,ξ) for $0 < t < \kappa$, $-\infty < \xi < \infty$, where κ equals the length of the free shear layer F2 from the stator to the free surface divided by $\sec\theta$. The functions ϕ_{f2}, u_{f2}, j_{yf2}, and $j_{\xi f2}$ depend on one parameter κ, so that they are no longer universal functions. There is a slot in the domain at $t = 1$ for $0 < \xi < \infty$ respesenting the two surfaces of the rotor, so that the variables need not be continuous at $t = 1$ for $\xi > 0$. Equations (9) and the boundary conditions (10a), (10b), and (11a) still apply. The condition (10b) applies for both sides of the slot at $t = 1$. The free-surface condition (10c) becomes

$$\frac{\partial\phi_{f2}}{\partial t} = 0, \quad \text{at } t = \kappa, \quad \text{for } -\infty < \xi < \infty, \tag{27}$$

while matching core regions C2 and C4 gives

$$\phi_{f2} \to t, \quad \text{as } \xi \to \infty, \quad \text{for } 0 < t < 1, \tag{28a}$$

$$\phi_{f2} \to 1, \quad \text{as } \xi \to \infty, \quad \text{for } 1 < t < \kappa. \tag{28b}$$

The separation of variables solution (12) applies for $-\infty < \xi < 0$ and $0 < t < \kappa$, with α_m replaced by

$$\alpha_m = [(2m + 1)\pi/4\kappa]^{1/2}.$$

The separation of variables solution (13) applies for $0 < \xi < \infty$ and $0 < t < 1$. For $0 < \xi < \infty$ and $1 < t < \kappa$, we introduce

$$\phi_{F2} = 1 + \sum_{k=0}^{\infty} \sin[2\gamma_k^2(t-1)]e^{-\gamma_k^2(t-1)} \times [P_k \cos(\gamma_k \xi) + Q_k \sin(\gamma_k \xi)], \quad (29)$$

where

$$\gamma_k = [(2k+1)\pi/4(\kappa-1)]^{1/2}.$$

The coefficients A_m, B_m, C_n, D_n, P_k, and Q_k are determined by minimizing the same residual E used in Sec. II, except that the limits of integration are from $t=0$ to $t=\kappa$.

Specific results for this new one-parameter free shear layer are not presented here. For $0<t\lesssim 1$, the velocity profiles are very similar to those in Fig. 3. As t increases from 1, the velocity profiles spread out and the peak velocity decreases, but with the constraint that

$$\int_{-\infty}^{\infty} u_{F1}\, d\xi = 1, \quad \text{for all } 1<t<\kappa.$$

As the left free surface rises from $y=1$ to $y=f_1(z)$, the free shear layer F1 simply follows the point $y=f_1(-b)$, $z=-b$ and the free-surface velocity is still zero, except near the rotor side. The only changes in the free shear layer F1 arises from changes in λ and ϕ_1. Some additional current flows between the stator and rotor through the new part of core C2. As the right free surface rises from $y=1$ to $y=f_2(z)$, a new core C4 with $u=1$ develops and the free shear layer F2 intersects the free surface. The free-surface velocity is 1 from the rotor side to the free shear layer, $\pm O(M^{-1/2})$ inside the free shear layer, and zero from the free shear layer to the stator side. The volume flux per unit $\Delta\eta$ in the free shear layer F2 increases linearly from zero at the stator to a value at the rotor corner and then keeps that constant value from the rotor corner to the free surface.

V. INSULATING LAYERS ON THE SIDES OF THE ROTOR OR STATOR

Here we present the extension of the analysis of Sec. IV to devices with thin layers of electrical insulators on the sides of the rotor at $z=\pm b$ or on the sides of the stator at $z=\pm(a+b)$. The thickness of the electrical insulators is assumed to be much smaller than $M^{-1/2}$, so that they are thinner than the free shear layers.

The subregions of the liquid metal for insulators on the sides of the rotor are shown in Fig. 6. The solution (6), neglecting $O(M^{-1})$ terms, again holds in core regions C1 and C3. The Hartmann layer adjacent to the insulator at $z=b$ must match the jump in u from zero in core C1 to 1 at the rotor surface. This Hartmann layer involves an $O(1)$ current density j_y and the circuit for this current must be completed through a free shear layer at $\xi=-b\cos\theta-f_1(-b)\sin\theta$, i.e., along the magnetic field line through the point where the free surface and insulator meet. This implies an $O(M^{-1/2})$ current density j_y inside this free shear layer, which in turn implies an $O(1)$ fluid velocity u. Thus this free shear layer is another weak layer involving only an $O(1)$ velocity.

The core region C2 occupies the same region and has the same solution (7), neglecting $O(M^{-1})$ terms, as in Sec. II. In the core C4,

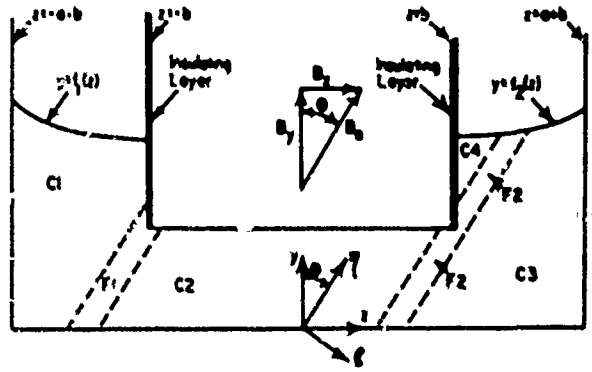

FIG. 6. Subregions of the liquid metal for $M\gg 1$ and thin electrical insulators on the sides of the rotor at $z=\pm b$. The Hartmann layers and a weak free shear layer at $\xi=-b\cos\theta-f_1(-b)\sin\theta$ are shown.

$u_x=1$, $\phi_x=C+\xi-b\cos\theta+\sin\theta$, $j_{yx}=j_{\xi x}=0$, neglecting $O(M^{-2})$ terms. The constant C is determined by matching the free shear layer F2.

The rescaling (8) and the boundary value problem (9)–(11) for the free shear layer F1 is the same as that presented in Sec. II, except that the free-surface condition (10c) is replaced by the solid insulator condition (14). Walker *et al.*[3,9] present the solution for this modified free shear layer: Although the analysis is much more complex, the results are surprisingly similar to those presented in Fig. 3.

The boundary value problem for the free shear layer F2 is the same as that presented in Sec. IV, except that the boundary condition on the top of the slot in the domain becomes

$$\frac{\partial\phi_{F2}}{\partial t}+\frac{\partial^2\phi_{F2}}{\partial\xi^2}=0, \quad \text{at } t=1^+, \quad \text{for } 0<\xi<\infty \quad (30)$$

and matching core C4 gives

$$\phi_{F2}\to C, \quad \text{as } \xi\to\infty, \quad \text{for } 1<t<\kappa. \quad (31)$$

The change from the boundary condition (10b) at $t=1^+$ to condition (30) precludes the relatively simple separation of variables solution discussed in Sec. IV. Without solving for this new layer, we can draw some conclusions about its solution. The integral of u_{F2} from $\xi=-\infty$ to $\xi=\infty$ equals the jump in ϕ_{F2} at each value of t. For $0<t<1$, this integral equals t, so that the velocity profiles here cannot deviate significantly from those in Fig. 3. With an insulator at $z=b$, there is no constant potential jump for $1<t<\kappa$, but the jump here must be independent of t, i.e., it must equal C. The jet for $1<t<\kappa$ and the associated potential jump C are driven by continuity of the electric potential ϕ_F and the electric current density $j_{yF}=-\partial\phi_F/\partial t$ at $t=1$ for $-\infty<\xi<0$. The velocity profiles may spread out as t increases from 1, but the total flow per unit Δt in each profile must be the same.

The effect of adding an insulating layer on the side of the rotor at $z=-b$ is to move the free shear layer F1 from the magnetic field line through the point $y=f_1(-b)$, $z=-b$ to the field line through the point $y=1$, $z=-b$. The strip of fluid between these two lines becomes stagnant and current free, except in the Hartmann layer at $z=-b$. The net electric current between the stator and rotor is once again

$2\phi_w \dot{\rho} \cos^2\theta$, as in Sec. II. The only effect of adding the insulating layer at $z = b$ is to slightly alter the velocity profiles inside the free shear layer F2.

Increasing the magnitude of $f_1(z)$ in Fig. 6 does not change anything. However, if $f_1(z)$ is increased sufficiently so that the free shear layer F2 intersects the stator rather than the free surface, then several changes occur in core C4 and the free shear layer F2. The C4 core solution with $u_r = 1$ still applies in the triangle formed by the insulator at $z = b$, the free surface at $y = f_2(z)$, and the magnetic field line through the point where the free surface and stator meet at $y = f_2(a+b)$, $z = a+b$. There is a new core C5 between this magnetic field line and the free shear layer F2, i.e., in the strip

$$(a+b)\cos\theta - f_2(a+b)\sin\theta < \xi < b\cos\theta - \sin\theta. \tag{32}$$

In this new core, $u_r = \phi_r = j_{w} = j_{\xi} = 0$, neglecting $O(M^{-2})$ terms. There is a weak free shear layer between cores C4 and C5. This weak layer matches the jump in u_r from zero in C5 to 1 in C4 and completes the circuit for $O(1)$ current density j_y in the Hartmann layer between the insulator at $z = b$ and core C5. In the boundary value problem for the free shear layer F2, conditions (27) and (31) are replaced by

$$\phi_{F2} = 0, \quad \text{at } t = \kappa, \quad \text{for } -\infty < \zeta < \infty, \tag{33a}$$

$$\phi_{F2} = 0, \quad \text{as } \zeta \to \infty, \quad \text{for } 1 < t < \kappa. \tag{33b}$$

Again, the velocity profiles for $0 < t < 1$ must closely resemble those presented in Fig. 3, but now the integral of u_y from $\zeta = -\infty$ to $\zeta = \infty$ must equal zero for $1 < t < \kappa$. The profile at $t = 1^+$ consists of $-u_f$ for $\zeta > 0$ and $+u_f$ for $\zeta < 0$, by continuity with the solution at $t = 1^-$. As t increases from 1, this basic character persists, but the magnitude of the velocity quickly decreases to zero. Therefore, for $t > 1$, there is a double jet with no net flow which is concentrated very near the rotor corner.

We now consider the addition of insulating layers on the sides of the stator at $z = \pm(a+b)$ to the situations shown in Figs. 5 and 6, i.e., with insulators only on the stator sides and on both the stator and rotor sides, respectively. For Figs. 5 and 6 we have assumed that $f_1(-b)$ is sufficiently small such that the magnetic field line through the point $y = f_1(-b)$, $z = -b$ intersects the stator at $y > 0$ and $f_2(a+b)$ is sufficiently small such that the free shear intersects the free surface. For these low free-surface locations, the addition of insulators at $z = \pm(a+b)$ has absolutely no effect on the solutions with or without insulators at $z = \pm b$.

If $f_1(-b)$ is increased, so that the magnetic field line through the point $y = f_1(-b)$, $z = -b$ intersects the insulated stator side at $z = -a-b$, then a new core C6 occurs between this magnetic field line and the field line through the corner $y = 0$, $z = -a-b$, i.e., in the strip

$$-b\cos\theta - f_1(-b)\sin\theta < \xi < -(a+b)\cos\theta. \tag{34}$$

The C1 solution, with $u_r = 0$, still applies in the triangle above $\xi = -b\cos\theta - f_1(-b)\sin\theta$.

If the side of the rotor at $z = -b$ is not insulated, then

$$u_r = 1, \quad \phi_r = \Psi(\xi), \quad j_{w} = j_{\xi r} = 0, \tag{35}$$

neglecting $O(M^{-2})$ terms, in the new core C6. The free shear layer F1 lies along the magnetic field line through the corner at $y = 0$, $z = -a-b$ and the C2 core solution applies to the right of the free shear layer. The solution of Walker *et al.*[8,9] applies to layer F1. The principal change is that the potential jump across this layer is now zero at the rotor surface at $t = 1$ and $\phi_1 = \phi_0 + \sin\theta - (a+b)\cos\theta$ at the stator corner at $t = 0$. The insulating free surface has moved above layer F1 and this layer now stems from the junction of the insulating and perfectly conducting stator walls. Therefore, the velocity profiles closely resemble those in Fig. 3 with t replaced by $(1-t)$. Moving in the $+y$ direction from the free shear layer F1, $u_r = 1$ in the new core C6; u decreases from 1 to zero inside the weak free shear layer along the magnetic field line through the point $y = f_1(-b)$, $z = -b$; and $u_r = 0$ in core C2 to the free surface.

We now consider the problem for a high left free surface with insulators at both $z = -a-b$ and $z = b$. The free shear layer F1 is in the position shown in Fig. 6 and its solution is unchanged by the addition of the insulator at $z = -a-b$. The C1 core solution with $u_r = \phi_r = j_{w} = j_{\xi r} = 0$, neglecting $O(M^{-2})$ terms, applies in the strip between the free shear layer F1 and the magnetic field line through the stator corner at $y = 0$, $z = -a-b$. The new core C6 occupies the strip defined by the limits (34) and has a solution

$$u_r = 0.5, \quad \phi_r = 0.5[\xi + (a+b)\cos\theta], \tag{36}$$

with $j_{w} = j_{\xi r} = 0$, neglecting $O(M^{-2})$ terms. By conservation of current, the j_y inside the Hartmann layers adjacent to the insulators at $z = -b$ and at $z = -a-b$ must be equal and opposite. Since the jump in u across these Hartmann layers is proportional to these currents, u_r is 0.5 between a moving and a fixed insulator. In the triangular core C1 above the magnetic field line through the point $y = f_1(-b)$, $z = b$,

$$\phi_r = 0.5a\cos\theta - 0.5f_1(-b)\sin\theta,$$

with $u_r = j_{w} = j_{\xi r} = 0$, neglecting $O(M^{-2})$ terms. Moving upward from layer F1, u is first zero; then 0.5; and finally, zero again.

With a high right free surface, the triangular core C4 extends to the stator at $z = a+b$ and there is a new core C5 between core C4 and the free layer F2, i.e., in the strip defined by the limits (32). In the cores C3 and C4, $u_r = 0$ and 1, respectively, with or without insulators on either side. If the stator side at $z = a+b$ is insulated, but the rotor side at $z = b$ is not insulated, then the solution (35) applies in the new core C5. Therefore, $u_r = 1$ throughout the axial gap above the free shear layer F2. The only distinction between cores C4 and C5 is that there is a weak free shear layer between them which completes the circuit for the j_y in the Hartmann layer between the new core C5 and the insulator at $z = a+b$. The boundary value problem for the free shear layer F2 is the same as that discussed in Sec. IV, except that the boundary condition (27) is replaced by

$$\frac{\partial\phi_{F2}}{\partial t} = \frac{\partial^2\phi_{F2}}{\partial\zeta^2}, \quad \text{at } t = \kappa, \quad \text{for } -\infty < \zeta < \infty. \tag{37}$$

This change precludes the separation of variables solutions presented in Sec. IV, but it does not change the fact that the integral of u_F from $\zeta = -\infty$ to $\zeta = \infty$ is 1 for all $1 < t < \kappa$.

If both sides at $z = b$ and $z = a + b$ are insulated, then the solution (36) with $\phi_c = 0.5\xi + C + \sin\theta - b\cos\theta$ applies in the new core C5. The constant C is determined by matching the free shear layer F2. As we move up the axial gap from layer F2, u_c first equals 0.5 in core C5 and then equals 1 in the core C4. The boundary value problem for the free shear layer F2 is the same as that discussed earlier in this section, except that the boundary condition (33a) is replaced by condition (37) and the matching condition (31) applies. Again, the integral of u_F from $\zeta = -\infty$ to $\zeta = \infty$ equals a constant C for all $1 < t < \kappa$, where C is different from that for an insulated rotor side and a perfectly conducting stator side and is determined by solving the free shear layer problem.

VI. CONCLUSIONS

This paper presents solutions for the primary azimuthal flow in liquid-metal current collectors for homopolar devices. If the local magnetic field is strong and has both radial and axial components, then an asymptotic analysis for large Hartmann numbers is appropriate. The solutions in the inviscid core regions are very simple. The solutions for the free shear layers along magnetic field lines through junctions of perfect conductors and insulators are either presented here or discussed. This asymptotic analysis leads to simple expressions for the net electric current and the power losses due to Joulean heating and viscous dissipation.

For a nearly axial magnetic field, the asymptotic analysis is not appropriate. Arbitrary Hartmann number solutions are presented for an axial magnetic field and axial free surfaces aligned with the rotor face at $y = 1$. This analysis can be extended to other axial free surfaces at $y = f_1 = f_2 = \text{const}$. One separation of variables solution is used for $0 < y < 1$, $0 < z < b$ and satisfies the boundary conditions at $y = 0$, $y = 1$, and $z = 0$. A second separation of variables solution applies for $0 < y < f_2$, $b < z < a + b$ and satisfies the boundary conditions at $y = 0$, $y = f_2$, and $z = a + b$. The residual is formed from the boundary conditions at $z = b$ for $1 < y = f_2$ and the continuity of u, $\partial u/\partial z$, h, and $\partial h/\partial z$ at $z = b$ for $0 < y < 1$. This method works for problems without any insulating layers or with insulating layers on the stator sides, or rotor sides, or both. This method can be extended to different free-surface locations, where f_1 and f_2 are different constants. The symmetry about $z = 0$ is then lost and the number of coefficients in the separation of variables solutions is doubled.

A typical value of the Reynolds number for the primary flow, $\mathrm{Re} = \rho UL/\mu$, is 12 000. At present, it is uncertain whether this flow is laminar or turbulent. An ordinary Couette flow with this Reynolds number would probably be turbulent. However, a strong magnetic field suppresses turbulence and increases the value of the critical Reynolds number. This magnetic suppression of turbulence depends on the electrical characteristics of the walls and is strongest with highly conducting walls which allow current circulations which damp the turbulent eddies. In addition, the gap is very small, so that wall damping is strong. These considerations would indicate that the flow is laminar. On the other hand, MHD effects lead to liquid-metal velocities which may be as large as $5U$ or may be negative, so that Re based on U and L may underestimate the largest velocity gradient in the flow. The velocity profile depends on the amount of electric current between the stator and rotor, so that the flow may be laminar for one current and turbulent for another. The laminarization of a turbulent flow by a strong magnetic field has been studied experimentally for flows in circular pipes and rectangular ducts, but these results may not apply for the present Couette flows in a very small gap with strong electromagnetic pumping; there is clearly a need for appropriate experiments.

ACKNOWLEDGMENTS

This research was supported by the Independent Research/Independent Exploratory Development (IR/IED) program at the David Taylor Research Center and by U.S. Navy Contract No. N6153387M0971.

[1] H. O. Stevens, M. J. Superczynski, T. J. Doyle, J. H. Harrison, and H. Messinger, IEEE Trans. Magn. 13, 269 (1977).
[2] J. Johnson, in *Proceedings of the 32nd IEEE Conference on Electric Contacts*, edited by the Components, Hybrids, and Manufacturing Technology Society (CHMT) of the Institute of Electrical and Electronics Engineers (IEEE, New York, 1986), p. 3.
[3] N. A. Sondergaard, P. J. Reilly, and V. H. Dilling, in *Proceedings of the 1987 Current Collector Conference* (Center for Electromechanics, Austin, TX, 1987).
[4] J. T. Woo, J. F. Pipkins, S. H. Brown, N. A. Sondergaard, and J. S. Walker, J. Appl. Phys. 63, 4872 (1988).
[5] L. N. Hjellming and J. S. Walker, J. Fluid Mech. 164, 237 (1986).
[6] W. E. Langlois and J. S. Walker, *Computational and Asymptotic Methods for Boundary and Interior Layers, Proceedings of the BAIL II Conference*, edited by J. J. H. Miller (Boole, London, 1982).
[7] J. C. R. Hunt and J. A. Shercliff, Annu. Rev. Fluid Mech. 3, 37 (1971).
[8] J. S. Walker, S. H. Brown, and N. A. Sondergaard, J. Appl. Phys. 64, 48 (1988).
[9] J. S. Walker, S. H. Brown, and N. A. Sondergaard, J. Appl. Phys. 64, 1736 (1988).

INITIAL DISTRIBUTION

Copies

12 DTIC

1 Dr. Ralph Burton
Mr. Gaines Burton
Burton Technologies Incorp.
4940 B North Boulevard
Raleigh, North Carolina 27606

20 Dr. John S. Walker
University of Illinois
at Urbana-Champaign
Department of Mechanical and
Industrial Engineering Building
1206 West Green St.
Urbana, Illinois 61801

20 Gita Talmage
University of Illinois
at Urbana-Champaign
Department of Mechanical and
Industrial Engineering Building
1206 West Green St.
Urbana, Illinois 61801

CENTER DISTRIBUTION

Copies	Code	Name
5	0113	Douglas
1	2702	Levedahl
1	2704	Quandt
2	271	Stevens
3	2710	Cox
3	2711	Smith
20	2712	Superczynski
1	2720	Urbach
1	5211	Knox
1	522.1	TIC (C)
1	522.2	TIC (A)
10	522.4	Report Control
2	5231	